Identification and Control of Electron-Nuclear Spin Defects in Diamond

Alexandre Cooper, Won Kyu Calvin Sun, Jean-Christophe Jaskula, and Paola Cappellaro

Identification and control of electron-nuclear spin defects in diamond

Alexandre Cooper,[1, 2] Won Kyu Calvin Sun,[1] Jean-Christophe Jaskula,[1] and Paola Cappellaro[1, *]

[1]*Department of Nuclear Science and Engineering and Research Lab of Electronics,
Massachusetts Institute of Technology, Cambridge, MA 02139, USA*
[2]*Department of Physics, Mathematics and Astronomy,
California Institute of Technology, Pasadena, CA 91125, USA*
(Dated: January 24, 2020)

We experimentally demonstrate an approach to scale up quantum devices by harnessing spin defects in the environment of a quantum probe. We follow this approach to identify, locate, and control two electron-nuclear spin defects in the environment of a single nitrogen-vacancy center in diamond. By performing spectroscopy at various orientations of the magnetic field, we extract the unknown parameters of the hyperfine and dipolar interaction tensors, which we use to locate the two spin defects and design control sequences to initialize, manipulate, and readout their quantum state. We finally create quantum coherence among the three electron spins, paving the way for the creation of genuine tripartite entanglement. This approach will be useful to assemble multi-spin quantum registers for applications in quantum sensing and quantum information processing.

Quantum devices that exploit the spins of impurity atoms or defect sites in solid-state materials offer promising applications in quantum communication [1–3], quantum information processing [4–6] and quantum sensing [7, 8]. Color centers with robust optical transitions and long-lived spin degrees of freedom are especially attractive to engineer optical networks of quantum registers [9–11] and atomic-scale sensors of time-varying magnetic fields [12–14]. The most studied of such color centers is the nitrogen-vacancy (NV) center in diamond, because of its outstanding optical and spin properties under ambient conditions [15].

An important problem with building scalable quantum devices based on synthetic NV centers is the existence of environmental spin defects, mostly byproducts of the NV creation process, such as nitrogen-related centers, vacancies, and their aggregates [16]. Whereas these spin defects usually cause fluctuations responsible for decoherence [17], they could rather serve as quantum resources were their spin properties under control [18, 19]. Although spin defects in the environment of a single NV center have been studied and controlled [20–26], a systematic approach to convert electron-nuclear spin defects into useful quantum resources is still needed, e.g., to transfer information between distant quantum registers [27–29] or improve the sensitivity of quantum sensors [19, 30–33].

Here, we experimentally demonstrate an approach to identify, locate, and control electron-nuclear spin defects in the environment of a quantum probe using double electron-electron resonance spectroscopy. Our approach relies on exploiting the non-trivial transformation of the spin Hamiltonian under rotation of the external magnetic field to estimate the parameters of the hyperfine and dipolar tensors, as needed to identify and locate unknown spin defects, as well as design control sequences to initialize, manipulate, and readout their quantum state. As a proof-of-principle demonstration, we spectrally charac-

terize two unknown electron-nuclear spin defects in the environment of a single NV center in diamond and create quantum coherence among the three electron spins. These results demonstrate a further step towards assembling large scale quantum registers using electron spins in solid.

Our experimental system consists of a single NV center interacting through magnetic dipole-dipole interaction with two electron-nuclear spin defects (X_1, X_2) randomly created by implanting ^{15}N ions through nanometer-sized apertures in an isotopically-purified diamond crystal [34]. Each X spin consists of an electronic spin $S = 1/2$ strongly-coupled to a nearby nuclear spin $I = 1/2$, giving rise to two resolved hyperfine doublets in the spin-echo double-resonance (SEDOR) spectrum (Fig. 1a) [35]. Each hyperfine transition can be selectively addressed using resonant microwave pulses with negligible crosstalk. Interestingly, the X spins are stable under optical illumination, enabling repetitive readout of their quantum state [33].

Our approach to solving the system identification problem consists in estimating the parameters of the spin Hamiltonian describing each of the two electron-nuclear spin defects,

$$\mathcal{H}(\theta, \phi) = \beta_e \, \underline{B} \cdot \underline{\underline{g}} \cdot \underline{S} + \underline{S} \cdot \underline{\underline{A}} \cdot \underline{I} - g_n \beta_n \, \underline{B} \cdot \underline{I}, \quad (1)$$

where $\underline{B} = \underline{B}(\theta, \phi)$ is the static magnetic field vector of norm B_0, $\underline{\underline{A}}$ is the hyperfine interaction tensor, $\underline{\underline{g}}$ (g_n) is the g tensor (g factor) of the electron (nuclear) spin, and β_e (β_n) is the Bohr (nuclear) magneton (we set $\hbar = 1$).

To extract the energy eigenvalues of $\mathcal{H}(\theta, \phi)$, we perform double-resonance spectroscopy for different orientations of the magnetic field (Fig. 1b) by translating and rotating a permanent magnet with respect to the diamond sample. However, simply measuring the resonance frequency of the NV electron spin on only one of its electronic spin transition, e.g., via cw-ESR in the $m_s \in \{0, -1\}$ manifold (Fig. 1c), is not sufficient to
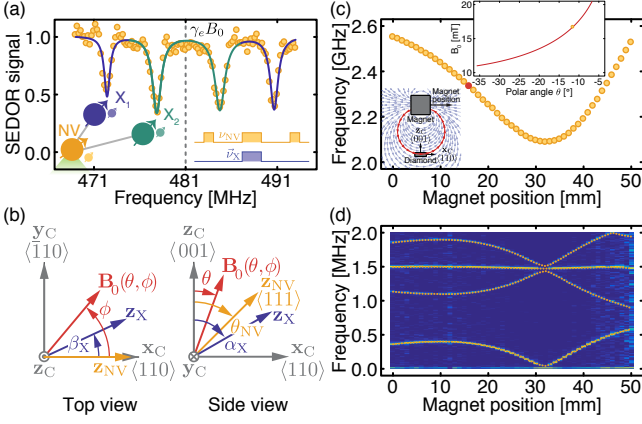
FIG. 1. **Identifying two unknown spin defects in diamond. (a)** A single nitrogen-vacancy center (NV) interacts with two electron-nuclear spin defects (X$_1$, X$_2$) in diamond. The spin-echo double-resonance (SEDOR) spectrum measured by applying a recoupling π pulse at a variable frequency $\vec{\nu}_\mathrm{X}$ during a spin-echo on the NV electron spin exhibits two resolved hyperfine doublets centered around the free-electron spin resonance frequency $\nu_e = \gamma_e B_0$, where γ_e is the gyromagnetic ratio of the free electron and $B_0 = 171.8$ G is the strength of the static magnetic field oriented along the molecular axis of the NV center. The solid line is a fit to four Lorentzian spectral lines associated with the two hyperfine resonances of X$_1$ (blue, outer spectral lines) and X$_2$ (green, inner spectral lines) **(b)** The unknown parameters of the hyperfine and dipolar tensors of the X spins are measured by varying the strength and orientation of the magnetic field using a permanent magnet. The polar and azimuthal angles parametrizing the orientation of the magnetic field (θ, ϕ) and the principal axes of the hyperfine tensors for the NV center ($\theta_\mathrm{NV} = 54.7°$, $\phi_\mathrm{NV} = 0°$) and X spins (α_X, β_X) are defined with respect to the crystallographic axes ($\mathbf{x}_C$, $\mathbf{y}_C$, $\mathbf{z}_C$) of the diamond crystal. **(c)** NV resonance frequency for various magnet positions. For each magnet position, there exist multiple values of the strength and orientation of the magnetic field that result in the same NV resonance frequency (inset). **(d)** Electron-spin-echo envelope modulation (ESEEM) spectroscopy of the NV center for various magnet positions. The spectral components at the nuclear frequencies result from hyperfine mixing with the host ^{15}N nuclear spin in the presence of a non-axial magnetic field. For each magnet position, the field strength (B_0) and polar angle (θ) are unambiguously determined by finding the simulated spectrum (dotted lines) that best matches the measured spectrum. The frequency wrapping for large magnet positions is an artifact of bandlimited sampling that is captured by our model.

uniquely characterize $\underline{B}(\theta,\phi)$ [36, 37]; there indeed exists multiple admissible pairs of (B_0,θ) resulting in the same resonance frequency (inset of Fig. 1c). To resolve this ambiguity, we measure the frequencies of the electron spin-echo envelope modulation (ESEEM) [38] caused by the strong dipolar coupling to the ^{15}N nuclear spin (Fig. 1d). When the magnetic field is misaligned with respect to the NV molecular axis ($\langle 111 \rangle$ crystallographic axis), the energy levels of the NV electron and
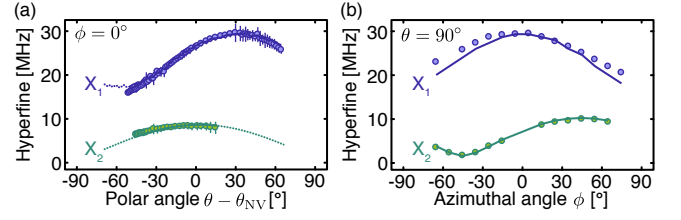

FIG. 2. **Characterizing the hyperfine tensors of two spin defects in diamond. (a)** Measured hyperfine strengths for various polar angles of the magnetic field (θ) plotted with respect to the polar angle of the NV center (θ_{NV}) in the azimuthal plane $\phi = 0°$. **(b)** Measured hyperfine strengths for various azimuthal angles of the static magnetic field (ϕ) in the polar plane $\theta = 90°$. The solid lines are the best least-square fit of both sets of data to the eigenvalues of an axially-symmetric hyperfine tensor with four free parameters.

nuclear spins are mixed, such that the spin-echo signal is modulated at the nuclear frequencies and their combinations, $\{\nu_1, \nu_0, \nu_1 \pm \nu_0\}$. Performing a numerical fit to the ESEEM spectrum [39], we unambiguously determine the magnetic field strength and polar angle at each magnet position [34].

To estimate the parameters of the hyperfine tensors, we follow an approach akin to tomographic imaging reconstruction. Geometrically, the hyperfine tensor can be represented as an ellipsoid, whose dimensions are given by the principal components, $\{A_x, A_y, A_z\}$, and principal angles, $\{\alpha_X, \beta_X, \gamma_X\}$, of the hyperfine tensor. Rotating the magnetic field around a fixed axis generates multiple tomographic cuts of the ellipsoid from which the hyperfine parameters can be estimated.

Specifically, we estimate the hyperfine parameters by monitoring the change in the hyperfine splitting of the X spins as a function of the orientation of the magnetic field (Fig. 2). To simplify the reconstruction problem, we assume the hyperfine tensors $\underline{\underline{A}}$ to be axially symmetric ($A_x = A_y \equiv A_\perp$), neglect the nuclear Zeeman term, and choose the g tensor to be isotropic with its principal value equal to the electron spin g-factor ($\underline{g} = g_e \cdot \underline{1}$). These assumptions are consistent with our measurements, which could be further extended to distinguish between an axially-symmetric tensor and a full tensor [34].

Characterizing the hyperfine tensor thus involves measuring a set of four unknown parameters, $\{A_\perp, A_\parallel, \alpha_X, \beta_X\}$, which we experimentally determine by simultaneously fitting the measured hyperfine strengths to the parametric equations for the eigenvalues of $\mathcal{H}(\theta,\phi)$. We thus obtain $A_\perp = 17.2(3)$, $A_\parallel = 29.4(2)$, $\alpha_X = 0(2)$, $\beta_X = 87(2)$ for X$_1$ and $A_\perp = 1.6(3)$, $A_\parallel = 11.2(2)$, $\alpha_X = 45(2)$, $\beta_X = 66(2)$ for X$_2$. We did not find any defects sharing these parameters in the literature [40–46], suggesting that they may never have been detected using conventional spectroscopy
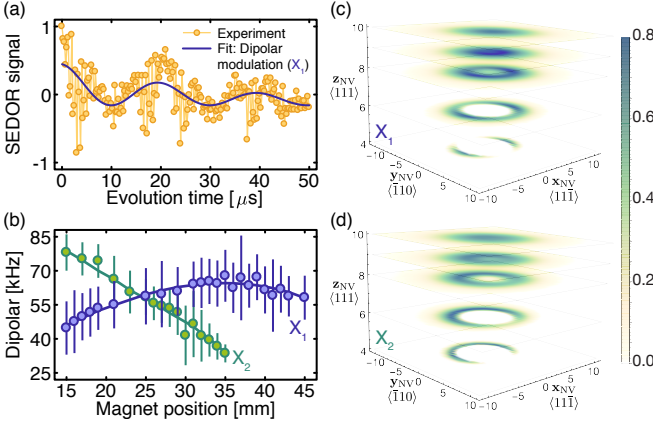
FIG. 3. **Locating two spin defects in diamond.** (a) Typical dipolar oscillations measured using a recoupled spin-echo sequence in the presence of a non-axial magnetic field. The slow modulation (solid blue line) is caused by the dipolar interaction between the NV electron spin and the X_1 electron spin, whereas the fast modulation is caused by the hyperfine mixing with the NV nuclear spin. (b) Measured dipolar coupling strengths between the NV electron spin and the X_1 (blue) and X_2 (green) electron spins for various magnet positions. The solid line is the best least-square fit to the eigenvalues of the interacting spin Hamiltonian with three free parameters (r, ζ, ξ, see [34]), which parametrize the relative position of the two X spins with respect to the NV center. (c-d) Probability distribution maps of the location of the X_1 (top) and X_2 (bottom) spins defined with respect to the coordinate frame of the NV center placed at the origin. The darker color indicates a higher probability of finding the X spin at this specific location.

methods. These defects are possibly nitrogen- or silicon-related centers resulting from nitrogen-ion implantation through a 10-nm amorphous SiO_2 layer introduced to mitigate ion channeling [47]. Further triple-resonance measurements on the X nuclear spins should enable unambiguous identification of the nuclear spin species.

To spatially locate the two defects, we measure the change in dipolar interaction strengths as we rotate the polar angle θ of the magnetic field in the azimuthal plane $\phi = 0$. Because the NV and X electron spins are quantized along different axes, the transformation of the dipolar interaction tensor under rotation of the magnetic field is non-trivial [34]. Another complication is that, as the magnetic field is rotated away from the NV molecular axis, the NV coherence signal becomes modulated by the hyperfine interaction with the ^{15}N nuclear spin, in addition to the desired modulation due to the dipolar interaction with the recoupled X electron spin (Fig. 3a).

To generate probability distribution maps for the location of the X spins with respect to the NV center (Fig. 3c-d), we evaluate the least-square error between the dipolar strengths computed for various admissible locations of the defects and the dipolar strengths measured from the low-frequency components of the SEDOR sig-
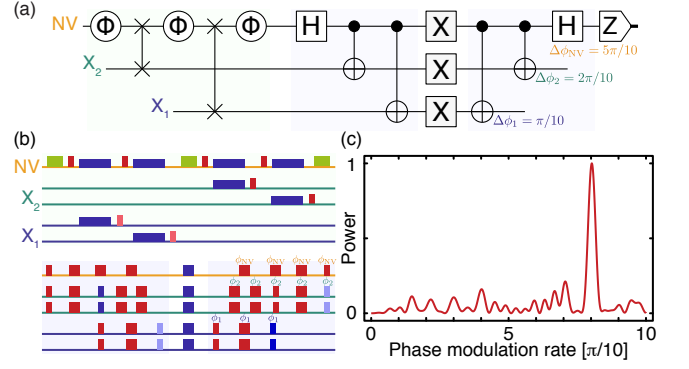

FIG. 4. **Creating and detecting three-spin coherence.** (a-b) The dissipative channel Φ removes entropy out of the quantum system by optically pumping the NV center (green box). The SWAP operations implemented using Hartmann-Hahn cross-polarization with $\pi/2$ pulses along the $\pm y$ axis (bright and pale red box) and continuous driving along the $\pm x$ axis (bright and pale blue box) exchange the state of the NV and X spins, effectively polarizing the X spins. A series of Hadamard (H) and CNOT gates implemented using $\pi/2$ and π pulses realize an entangling and disentangling gate to create and detect three-spin coherence, which is protected against dephasing by a series of X gates. The three-spin coherence is mapped back into a population state of the NV spin using a series of disentangling gates and measured projectively in the Z basis (green box). The phase of the pulses of the disentangling gate on the NV, X_1, and X_2 spins are incremented by steps of $\Delta\phi_{NV} = 5\pi/10$, $\Delta\phi_2 = 2\pi/10$, and $\Delta\phi_1 = \pi/10$ respectively to spectrally label the spin coherence terms. (c) The power spectrum of the the signal shows parity oscillations [48] at the sum of the three modulation rates ($\Delta\phi_\Sigma = 8\pi/10$), thus indicating the creation of three-spin coherence [34].

nal (Fig. 3b). At the most probable location, we estimate the distance from the NV center to be $r_1 = 9.23(3)$ nm and $r_2 = 6.58(3)$ nm for X_1 and X_2 respectively. We searched for signatures of coherent interaction between X_1 and X_2, but could not resolve any, indicating that the two defects are farther apart to each other than to the NV center.

Having partially identified and located the two X defects, we now have a consistent description of the three-spin system that is sufficient to design control protocols to engineer its quantum state and create correlated states of multiple spins. To demonstrate control of the two X spins [34], we create quantum coherence among the three electron spins, taking a first step towards the creation of genuine tripartite entanglement. Our control protocol (Fig. 4) is based on (1) initializing the three-spin system in a pure state using coherent spin-exchange with the optically-polarized NV spin, (2) creating three-spin coherence using a series of entangling CNOT gates, and (3) mapping the coherence back into a population difference on the NV spin using a series of disentangling CNOT gates with modulated phases.

Specifically, because the X spins lacks a known mechanism for dissipative state preparation, we first initialize its quantum state using multiple rounds of Hartmann-Hahn cross-polarization [49–51], which relies on simultaneously driving both spins at the same Rabi frequency to engineer coherent spin exchange in the rotating frame at a rate given by the dipolar coupling strength.

We then create three-spin coherence by synthesizing entangling gates using the recoupled spin-echo sequence [35], which decouples the NV spin from its environment using a spin-echo sequence while selectively recoupling the dipolar interaction with the X spin with a recoupling π pulse. The recoupled spin-echo sequence correlates the two spins, but does not necessarily create entanglement in the presence of control imperfections.

We finally quantify the amount of three-spin coherence created after the entangling gate by mapping it back into a measurable population difference on the NV spin. To distinguish between the creation of single-spin and multi-spin coherence, we increment the phase of the pulses of the disentangling gates after each realization of the experiment by steps of $5\pi/10$, $2\pi/10$, and $\pi/10$ for the NV, X_1, and X_2 spins respectively. Although this method [52, 53] does not provide full state tomography, the modulation of the phases results in a modulation of the polarization signal (Fig. 4c) at a rate given by the sum of the three increment rates ($8\pi/10$), thus indicating the creation of three-spin coherence without significant leakage to other coherence terms and showing a first step towards the creation of genuine tripartite entanglement, which could be used to achieve quantum-enhanced sensing [33].

In conclusion, we have demonstrated an approach to identify and control electron-nuclear spin defects in the environment of a quantum probe using double-resonance spectroscopy. This approach will be useful to characterize unknown spin defects in solids so as to better understand their formation mechanisms, mitigate their detrimental influence, and harness their favorable spin, charge, and optical properties. This approach will also be useful to identify spin systems of greater complexity, including unknown molecular structures placed near the surface of diamond [30, 31]. Instead of more abundant species such as substitutional nitrogen defects (P1 centers) and free electrons, harnessing proximal electron-nuclear spin defects will enable better spectral separability in crowded spectrum and better stability against photoionization. Controlling their nuclear spins, e.g., by direct driving at the Larmor frequency using radio-frequency pulses in triple-resonance experiments, will provide further access to quantum resources to process and store quantum information.

––––––––––––

* pcappell@mit.edu
[1] L. Childress and R. Hanson, *MRS Bulletin*, **38**, 134 (2013).
[2] W. B. Gao, A. Imamoglu, H. Bernien, and R. Hanson, Nature Photonics **9**, 363 (2015).
[3] M. Atatüre, D. Englund, N. Vamivakas, S.-Y. Lee, and J. Wrachtrup, Nat. Mat. **3**, 38 (2018).
[4] J. J. L. Morton and B. W. Lovett, Annual Review of Condensed Matter Physics **2**, 189 (2011).
[5] D. D. Awschalom, L. C. Bassett, A. S. Dzurak, E. L. Hu, and J. R. Petta, Science **339**, 1174 (2013).
[6] T. F. Watson, B. Weber, Y.-L. Hsueh, L. C. L. Hollenberg, R. Rahman, and M. Y. Simmons, Science Advances **3**, e1602811 (2017).
[7] C. L. Degen, F. Reinhard, and P. Cappellaro, Rev. Mod. Phys. **89**, 035002 (2017).
[8] F. Casola, T. van der Sar, and A. Yacoby, Nature Reviews Materials **3**, 17088 (2018).
[9] H. J. Kimble, Nature **453**, 1023 (2008).
[10] H. Bernien, B. Hensen, W. Pfaff, G. Koolstra, M. S. Blok, L. Robledo, T. H. Taminiau, M. Markham, D. J. Twitchen, L. Childress, and R. Hanson, Nature **497**, 86 (2013).
[11] P. C. Humphreys, N. Kalb, J. P. J. Morits, R. N. Schouten, R. F. L. Vermeulen, D. J. Twitchen, M. Markham, and R. Hanson, Nature **558**, 268 (2018).
[12] J. M. Taylor, P. Cappellaro, L. Childress, L. Jiang, D. Budker, P. R. Hemmer, A. Yacoby, R. Walsworth, and M. D. Lukin, Nat. Phys. **4**, 810 (2008).
[13] A. Cooper, E. Magesan, H. Yum, and P. Cappellaro, Nat. Commun. **5**, 3141 (2014).
[14] A. Ajoy, U. Bissbort, M. D. Lukin, R. L. Walsworth, and P. Cappellaro, Phys. Rev. X **5**, 011001 (2015).
[15] M. W. Doherty, N. B. Manson, P. Delaney, F. Jelezko, J. Wrachtrup, and L. C. Hollenberg, Physics Reports **528**, 1 (2013).
[16] P. Deák, B. Aradi, M. Kaviani, T. Frauenheim, and A. Gali, Phys. Rev. B **89**, 075203 (2014).
[17] G. de Lange, Z. H. Wang, D. Riste, V. V. Dobrovitski, and R. Hanson, Science **330**, 60 (2010).
[18] L. Schlipf, T. Oeckinghaus, K. Xu, D. B. R. Dasari, A. Zappe, F. F. de Oliveira, B. Kern, M. Azarkh, M. Drescher, M. Ternes, K. Kern, J. Wrachtrup, and A. Finkler, Science Advances **3**, e1701116 (2017).
[19] G. Goldstein, P. Cappellaro, J. R. Maze, J. S. Hodges, L. Jiang, A. S. Sorensen, and M. D. Lukin, Phys. Rev. Lett. **106**, 140502 (2011).
[20] R. J. Epstein, F. M. Mendoza, Y. K. Kato, and D. D. Awschalom, Nat. Phys. **1**, 94 (2005).
[21] R. Hanson, F. M. Mendoza, R. J. Epstein, and D. D. Awschalom, Phys. Rev. Lett. **97**, 087601 (2006).
[22] F. Shi, Q. Zhang, B. Naydenov, F. Jelezko, J. Du, F. Reinhard, and J. Wrachtrup, Phys. Rev. B **87**, 195414 (2013).
[23] A. O. Sushkov, N. Chisholm, I. Lovchinsky, M. Kubo, P. K. Lo, S. D. Bennett, D. Hunger, A. Akimov, R. L. Walsworth, H. Park, and M. D. Lukin, Nano Letters **14**, 6443 (2014).

[24] M. Grinolds, M. Warner, K. De Greve, Y. Dovzhenko, L. Thiel, R. Walsworth, S. Hong, P. Maletinsky, and A. Yacoby, Nat. Nanotech. **9**, 279 (2014).

[25] H. S. Knowles, D. M. Kara, and M. Atatüre, Phys. Rev. Lett. **117**, 100802 (2016).

[26] E. L. Rosenfeld, L. M. Pham, M. D. Lukin, and R. L. Walsworth, Phys. Rev. Lett. **120**, 243604 (2018).

[27] P. Neumann, R. Kolesov, B. Naydenov, J. Beck, F. Rempp, M. Steiner, V. Jacques, G. Balasubramanian, M. L. Markham, D. J. Twitchen, S. Pezzagna, J. Meijer, J. Twamley, F. Jelezko, and J. Wrachtrup, Nat. Phys. **6**, 249 (2010).

[28] P. Cappellaro, L. Viola, and C. Ramanathan, Phys. Rev. A **83**, 032304 (2011).

[29] N. Y. Yao, L. Jiang, A. V. Gorshkov, Z.-X. Gong, A. Zhai, L.-M. Duan, and M. D. Lukin, Phys. Rev. Lett. **106**, 040505 (2011).

[30] F. Shi, Q. Zhang, P. Wang, H. Sun, J. Wang, X. Rong, M. Chen, C. Ju, F. Reinhard, H. Chen, J. Wrachtrup, J. Wang, and J. Du, Science **347**, 1135 (2015).

[31] I. Lovchinsky, A. O. Sushkov, E. Urbach, N. P. de Leon, S. Choi, K. De Greve, R. Evans, R. Gertner, E. Bersin, C. Müller, L. McGuinness, F. Jelezko, R. L. Walsworth, H. Park, and M. D. Lukin, Science **351**, 836 (2016).

[32] D. A. Simpson, R. G. Ryan, L. T. Hall, E. Panchenko, S. C. Drew, S. Petrou, P. S. Donnelly, P. Mulvaney, and L. C. L. Hollenberg, Nat. Commun. **8**, 458 (2017).

[33] A. Cooper, W. K. C. Sun, J.-C. Jaskula, and P. Cappellaro, Phys. Rev. Applied **12**, 044047 (2019).

[34] See Supplemental Material for details of the experiment and theoretical models, which includes Refs. [54, 55].

[35] G. de Lange, T. van der Sar, M. Blok, Z.-H. Wang, V. Dobrovitski, and R. Hanson, Scientific Reports **2**, 382 EP (2012).

[36] G. Balasubramanian, I. Y. Chan, R. Kolesov, M. Al-Hmoud, J. Tisler, C. Shin, C. Kim, A. Wojcik, P. R. Hemmer, A. Krueger, T. Hanke, A. Leitenstorfer, R. Bratschitsch, F. Jelezko, and J. Wrachtrup, Nature **455**, 648 (2008).

[37] S.-Y. Lee, M. Niethammer, and J. Wrachtrup, Phys. Rev. B **92**, 115201 (2015).

[38] W. B. Mims, Phys. Rev. B **5**, 2409 (1972).

[39] S. Stoll and A. Schweiger, J. Mag. Res. **178**, 42 (2006).

[40] J. H. N. Loubser and J. A. van Wyk, Reports on Progress in Physics **41**, 1201 (1978).

[41] J. Isoya, H. Kanda, Y. Uchida, S. C. Lawson, S. Yamasaki, H. Itoh, and Y. Morita, Phys. Rev. B **45**, 1436 (1992).

[42] J. A. van Wyk, O. D. Tucker, M. E. Newton, J. M. Baker, G. S. Woods, and P. Spear, Phys. Rev. B **52**, 12657 (1995).

[43] S. Felton, A. M. Edmonds, M. E. Newton, P. M. Martineau, D. Fisher, D. J. Twitchen, and J. M. Baker, Phys. Rev. B **79**, 075203 (2009).

[44] S. Liggins, M. E. Newton, J. P. Goss, P. R. Briddon, and D. Fisher, Phys. Rev. B **81**, 085214 (2010).

[45] M. K. Atumi, J. P. Goss, P. R. Briddon, F. E. Shrif, and M. J. Rayson, Journal of Physics: Condensed Matter **25**, 065802 (2013).

[46] B. L. Green, M. W. Dale, M. E. Newton, and D. Fisher, Phys. Rev. B **92**, 165204 (2015).

[47] D. M. Toyli, C. D. Weis, G. D. Fuchs, T. Schenkel, and D. D. Awschalom, Nano letters **10**, 3168 (2010).

[48] T. Monz, P. Schindler, J. T. Barreiro, M. Chwalla, D. Nigg, W. A. Coish, M. Harlander, W. Hänsel, M. Hennrich, and R. Blatt, Phys. Rev. Lett. **106**, 130506 (2011).

[49] S. R. Hartmann and E. L. Hahn, Phys. Rev. **128**, 2042 (1962).

[50] C. Belthangady, N. Bar-Gill, L. M. Pham, K. Arai, D. Le Sage, P. Cappellaro, and R. L. Walsworth, Phys. Rev. Lett. **110**, 157601 (2013).

[51] A. Laraoui and C. A. Meriles, ACS Nano **7**, 3403 (2013).

[52] W. Scherer and M. Mehring, J. Chem. Phys. **128**, 052305 (2008).

[53] M. Mehring, J. Mende, and W. Scherer, Phys. Rev. Lett. **90**, 153001 (2003).

[54] A. Acin, D. Bruss, M. Lewenstein, and A. Sanpera, Phys. Rev. Lett. **87**, 040401 (2001).

[55] R. Rahimi, A. Saitoh, M. Nakahara, and M. Kitagawa, Phys. Rev. A **75**, 032317 (2007).